



Article

K_{Ca}1.1 K⁺ Channel Inhibition Overcomes Resistance to Antiandrogens and Doxorubicin in a Human Prostate Cancer LNCaP Spheroid Model

Susumu Ohya * , Junko Kajikuri , Kyoko Endo, Hiroaki Kito and Miki Matsui

Department of Pharmacology, Graduate School of Medical Sciences, Nagoya City University, Nagoya 467-8601, Japan; kajikuri@med.nagoya-cu.ac.jp (J.K.); k.endo@med.nagoya-cu.ac.jp (K.E.); kito@med.nagoya-cu.ac.jp (H.K.); miki.matsui.4238@gmail.com (M.M.)

* Correspondence: sohya@med.nagoya-cu.ac.jp; Tel.: +81-52-853-8149

Abstract: Several types of K⁺ channels play crucial roles in tumorigenicity, stemness, invasiveness, and drug resistance in cancer. Spheroid formation of human prostate cancer (PC) LNCaP cells with ultra-low attachment surface cultureware induced the up-regulation of cancer stem cell markers, such as NANOG, and decreased the protein degradation of the Ca²⁺-activated K⁺ channel K_{Ca}1.1 by down-regulating the E3 ubiquitin ligase, FBXW7, compared with LNCaP monolayers. Accordingly, K_{Ca}1.1 activator-induced hyperpolarizing responses were larger in isolated cells from LNCaP spheroids. The pharmacological inhibition of K_{Ca}1.1 overcame the resistance of LNCaP spheroids to antiandrogens and doxorubicin (DOX). The protein expression of androgen receptors (AR) was significantly decreased by LNCaP spheroid formation and reversed by K_{Ca}1.1 inhibition. The pharmacological and genetic inhibition of MDM2, which may be related to AR protein degradation in PC stem cells, revealed that MDM2 was responsible for the acquisition of antiandrogen resistance in LNCaP spheroids, which was overcome by K_{Ca}1.1 inhibition. Furthermore, a member of the multidrug resistance-associated protein subfamily of ABC transporters, MRP5 was responsible for the acquisition of DOX resistance in LNCaP spheroids, which was also overcome by K_{Ca}1.1 inhibition. Collectively, the present results suggest the potential of K_{Ca}1.1 in LNCaP spheroids, which mimic PC stem cells, as a therapeutic target for overcoming antiandrogen- and DOX-resistance in PC cells.

Keywords: cancer spheroid model; K_{Ca}1.1; prostate cancer; cancer stemness; antiandrogen resistance; MDM2



Citation: Ohya, S.; Kajikuri, J.; Endo, K.; Kito, H.; Matsui, M. K_{Ca}1.1 K⁺ Channel Inhibition Overcomes Resistance to Antiandrogens and Doxorubicin in a Human Prostate Cancer LNCaP Spheroid Model. *Int. J. Mol. Sci.* **2021**, *22*, 13553. <https://doi.org/10.3390/ijms222413553>

Academic Editors: Niels Decher and Aytug Kiper

Received: 29 November 2021

Accepted: 13 December 2021

Published: 17 December 2021

Publisher's Note: MDPI stays neutral with regard to jurisdictional claims in published maps and institutional affiliations.



Copyright: © 2021 by the authors. Licensee MDPI, Basel, Switzerland. This article is an open access article distributed under the terms and conditions of the Creative Commons Attribution (CC BY) license (<https://creativecommons.org/licenses/by/4.0/>).

1. Introduction

Androgen deprivation therapy (ADT) is the standard care for the initial management of advanced and metastatic prostate cancer (PC); however, progression to castration-resistant PC (CRPC) occurs within a few years of the initiation of ADT [1]. The agents currently available for the treatment of CRPC include (1) chemotherapy agents, such as docetaxel (DTX), and (2) antiandrogens, including bicalutamide (BCT) and enzalutamide (EZT) [2,3]. However, PC patients with metastatic CRPC eventually become resistant to these agents [2,3]. CRPC under ADT causes genetic changes in androgen receptors (AR), such as overexpression, mutations, and splice variants [4]. Moreover, CRPC is also driven from PC stem cells (PCSCs), and the sustained prevention of AR protein expression by their degradation is one potential mechanism by which PCSCs acquire antiandrogen resistance [5]. Recently, poly (ADP-ribose) polymerase (PARP) inhibitors, such as olaparib, novel AR antagonists, such as darolutamide, and radio-ligand therapy with lutetium prostate-specific membrane antigen (Lu-PSMA) have emerged as potentially effective therapeutic options in patients with CRPC [6].

Multicellular tumor three-dimensional (3D) spheroid models are spherical self-assembled aggregates of cancer cells. They are a valuable tool for studying the tumor microenvi-

ronment (TME) in solid tumors and are also important for investigating the characteristics of CSCs, such as tumor initiation, metastasis, and resistance to chemotherapies (chemoresistance) [7,8]. Previous studies demonstrated that the expression of CSC markers, such as CD44 and NANOG, was upregulated in aggregated PC spheroid models and contributed to their acquisition of chemoresistance and antiandrogens [9,10]. Ultra-low attachment plates and dishes pre-coated with an ultra-hydrophilic polymer promoted the spontaneous formation of cancer spheroids.

Ion channels contribute to tumorigenicity, stemness, invasiveness, and chemoresistance in several cancers, including PC [11,12]. Recent studies have focused on the potential contribution of K^+ channels to cancer progression in TME and to the acquisition of therapy resistance [13,14]. The large-conductance Ca^{2+} -activated K^+ channel $K_{Ca}1.1$ encoded by *KCNMA1* overexpresses in PC and enhances the proliferative and metastatic abilities of PC cells through modifications of Ca^{2+} signaling [15,16]. The expression of $K_{Ca}1.1$ is regulated by transcriptional, epigenetic, and post-translational modifications in cancers [17,18]. The functional diversity of $K_{Ca}1.1$ also arises from alternative splicing and modifications by non-pore-forming regulatory molecules, such as β and γ subunits [19].

Post-translational modifications by E3 ubiquitin ligases (E3s) play a crucial role in protein stabilization, and the dysregulation of ubiquitination is associated with cancer progression, metastasis, and therapy resistance [20]. In sarcoma spheroid models, the downregulation of F-box/WD repeat-containing protein 7 (FBXW7) decreased the protein degradation of $K_{Ca}1.1$, which increased $K_{Ca}1.1$ activity [21]. Cereblon (CRBN) plays an important role in the assembly and plasma membrane expression of functional $K_{Ca}1.1$ [22] and also promotes AR protein degradation in androgen-sensitive human PC cell line, LNCaP [23]. In PCSCs, murine double minute 2 (MDM2) causes the sustained loss of AR protein expression by promoting the constant degradation of AR [24].

ATP-binding cassette (ABC) transporters, such as multidrug resistance (MDR/ABCB) and multidrug resistance-associated proteins (MRP/ABCC), are essential for the acquisition of chemoresistance [25]. MDR1 and MDR3 were previously shown to be involved in the acquisition of resistance to paclitaxel (PTX) and doxorubicin (DOX), respectively, while MRP1, MRP2, and MRP5 play a role in the acquisition of resistance to DOX and/or cisplatin (CIS) [26]. MRP4 is involved in the acquisition of resistance to DTX, but not to PTX, DOX, or CIS [26].

In the present study, human PC spheroid models with antiandrogen resistance were obtained from a LNCaP cell line *in vitro* using ultra-low attachment cultureware. The main objective of the present study is to elucidate the mechanisms underlying the acquired resistance to antiandrogens as it is overcome by the inhibition of $K_{Ca}1.1$ using a LNCaP spheroid model.

2. Results

2.1. Increased $K_{Ca}1.1$ Activity in the LNCaP Spheroid Model

The androgen-sensitive LNCaP functionally expresses $K_{Ca}1.1$ and the auxiliary γ subunit, leucine-rich repeat-containing protein 26 (LRRC26) promotes the activation of $K_{Ca}1.1$ at physiological voltages and Ca^{2+} levels [27]. Furthermore, the other commercially-available human PC cell lines, VCaP, PC-3, and DU-145, rarely expressed $K_{Ca}1.1$. Spheroidal aggregates of LNCaP cells were formed 5–7 days after cell seeding onto the ultra-low attachment cultureware (day 7, lower panel, Figure 1A). Hyperpolarizing responses induced by NS1619 (1 μ M), a $K_{Ca}1.1$ activator, were significantly larger in isolated cells from 3D spheroids on day 7 ('3D') than in those from 2D adherent cell monolayers ('2D') ($p < 0.05$) (Figure 1B,C). A pretreatment with the selective $K_{Ca}1.1$ blocker, paxilline (PAX) (1 μ M), almost reduced NS1619-induced hyperpolarizing responses (Supplementary Figure S1A,B). The expression level of the $K_{Ca}1.1$ protein increased by approximately four-fold in lipid-raft fractions (RIPA-insoluble, ultra-RIPA-soluble fractions) of LNCaP spheroids ($p < 0.05$) (Figure 1D,E), without changes in that of the $K_{Ca}1.1$ transcript ($p > 0.05$) (Figure 1F). Similarly, the flow cytometric analysis using the Alexa Fluor 488-conjugated anti- $K_{Ca}1.1$ an-

tibody showed that the relative mean intensity of Alexa Fluor 488 was approximately 4.5-fold higher in LNCaP cells from '3D' than '2D' (Supplementary Figure S1C). Moreover, the expression levels of the cancer stemness markers, NANOG [28], CD44, and KLF4, were markedly higher in 3D spheroids than in 2D monolayers (Figure 2). Among six auxiliary β and γ subunits, LRRC26 was predominantly expressed in both LNCaP monolayers and spheroids (Supplementary Figure S1D,E). We measured outward K^+ currents elicited in 3D-cultured LNCaP cells by depolarizing voltage steps between -80 and $+60$ mV from a holding potential of -60 mV using whole-cell patch-clamp recordings. Outward K^+ currents were completely blocked by the application of $1 \mu\text{M}$ PAX (Supplementary Figure S2A–C).

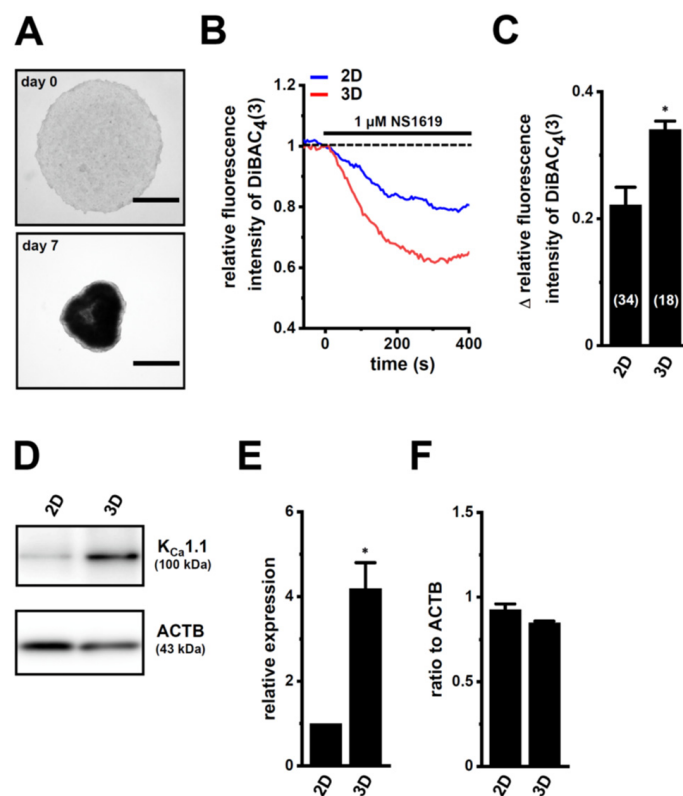


Figure 1. Comparison of $K_{Ca}1.1$ expression and activity between LNCaP cells cultured as 2D monolayers and 3D spheroids. (A): Phenotypic properties of LNCaP cells cultured in ultra-low attachment PrimeSurface 96U plates (upper panel: on day 0; lower panel: on day 7). Brightfield images were obtained with the Axio Observer Z1 microscope system (Carl Zeiss, Oberkochen, Germany). Bars show $500 \mu\text{m}$. (B): Time course of the voltage-sensitive fluorescent dye imaging of $K_{Ca}1.1$ activator ($1 \mu\text{M}$ NS1619)-induced hyperpolarizing responses in isolated cells from '2D' monolayers and '3D' spheroids of LNCaP. The fluorescent intensity of DiBAC₄(3) before the application of NS1619 is expressed as 1.0. Images were measured every 5 s. (C): Summarized results of NS1619-induced hyperpolarizing responses in cells isolated from at least three different batches in each group. Cell numbers used in experiments are shown in parentheses. The values for fluorescent intensity were obtained by measuring the average for 1 min (12 images). (D): $K_{Ca}1.1$ protein expression in the lipid-raft-enriched protein lysates of both groups. Blots were probed with anti- $K_{Ca}1.1$ (approximately 100 kDa, upper panel) and anti-ACTB (43 kDa, lower panel) antibodies. (E): Summarized results were obtained as the optical density of $K_{Ca}1.1$ and ACTB band signals. After compensation for the optical density of the $K_{Ca}1.1$ protein band signal with that of the ACTB signal, the $K_{Ca}1.1$ signal in '2D' was expressed as 1.0 ($n = 4$ for each). (F): Real-time PCR examination of $K_{Ca}1.1$ in both groups ($n = 4$ for each). Expression levels were shown as a ratio to ACTB. *: $p < 0.05$ vs. '2D'.

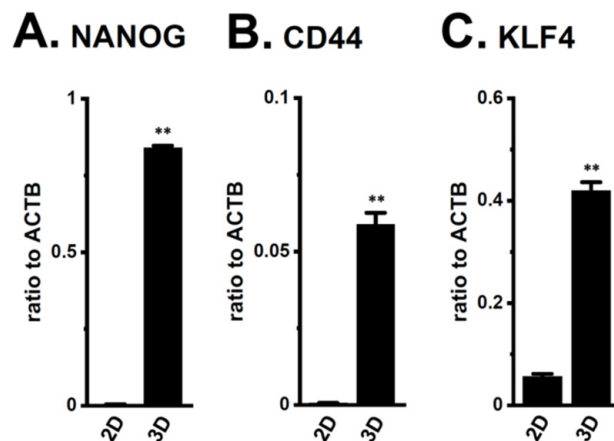


Figure 2. Expression of the transcripts of cancer stem markers, NANOG, CD44, and KLF4, in both 2D- and 3D-cultured LNCaP cells. (A–C): Real-time PCR examination of NANOG, CD44, and KLF4 in both groups ($n = 4$ for each). Expression levels were shown as a ratio to ACTB. **: $p < 0.01$ vs. '2D'.

2.2. Acquired Resistance of LNCaP Spheroids to Antiandrogens and DOX Overcome by $K_{Ca}1.1$ Inhibition

The optimization of the initial cell seeding density is essential for the WST-1 cell proliferation assay. Especially, it affects various parameters, such as metabolic activity and drug penetration in a 3D spheroid. Under the condition described in Section 4.2. (10^5 cells/mL at day 0), LNCaP cells cultured in a 2D monolayer almost doubled every 24 h from day 0 to day 3. Moreover, the metabolic activity of the WST-1 reagent in cells cultured in a 3D spheroid was reduced by almost 30% in 2 days; however, it was kept for the additional 7 days. We further examined the WST-1 assay in 3D spheroids with the different initial cell densities (2×10^4 , 5×10^4 , 10^5 , 2×10^5 , and 5×10^5 cells/mL); however, the drug sensitivities were almost same among them. As shown in Figure 3A–D, LNCaP spheroids acquired chemoresistance to DTX, PTX, DOX, and CIS following exposure for 48 h ($p < 0.01$). In LNCaP spheroids, the resistance to DOX alone was reversed by the pretreatment with $10 \mu\text{M}$ PAX for 24 h ($p < 0.01$) (Figure 3E–H). No significant changes in cell viability were found by the treatment with PAX alone for 48 h (1.032 ± 0.029 in relative cell viability ($n = 5$, $p > 0.05$)).

LNCaP spheroids also exhibited resistance to the antiandrogens BCT and EZT ($p < 0.01$) (Figure 4A,B). The PAX pretreatment significantly reversed the antiandrogen resistance acquired by LNCaP spheroids ($p < 0.01$) (Figure 4C,D). These results suggest that the inhibition of $K_{Ca}1.1$ may represent a novel strategy for overcoming antiandrogen resistance in patients with CRPC.

Among the 10 ABC transporter candidates (MDR1, MDR3, MRP1–6, and ABCG1–2) possibly involved in chemoresistance, the MRP1, 3, 4, and 5 transcripts were expressed at high levels in LNCaP spheroids, with the levels of transcripts other than MRP4 significantly increasing with the spheroid formation (Figure 5A–D). The expression levels of the other candidates were much lower in LNCaP spheroids (less than 0.002 in arbitrary units to ACTB). As shown in Figure 5E–H, the PAX treatment for 24 h significantly reversed the expression of MRP5 only. Western blot (WB) examinations also showed that increases in MRP5 protein expression levels in LNCaP spheroids were significantly reduced by the PAX treatment ($p < 0.05$) (Supplementary Figure S3A–D). No significant changes in MRP1, MRP3, and MRP4 protein expression levels were found by the PAX treatment (Supplementary Figure S4).

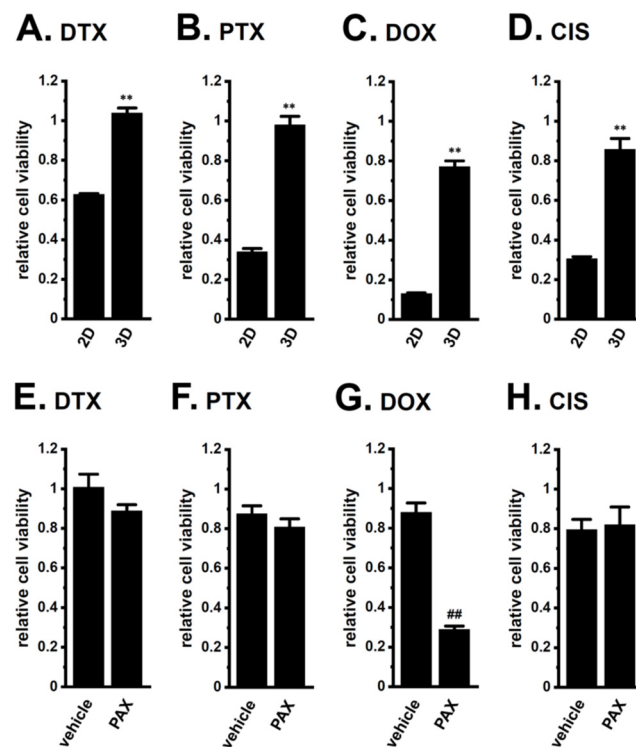


Figure 3. Effects of chemotherapy agents on the viability of 2D- and 3D-cultured LNCaP cells and the effects of a pretreatment with a $K_{Ca}1.1$ inhibitor on chemoresistance acquired by 3D-cultured LNCaP cells. (A–D): Effects of the treatment with 100 nM DTX, 100 nM PTX, 1 μ M DOX, and 10 μ M CIS for 48 h on the viability of '2D'- and '3D'-cultured LNCaP cells using the WST-1 assay ($n = 5$ for each). Cell viability adding 0.1% dimethylsulfoxide, DMSO in DTX, PTX, and DOX and water in CIS instead of chemotherapy agents was expressed as 1.0. (E–H): Effects of the treatment with chemotherapy agents for 48 h on the viability of vehicle- and 10 μ M PAX-pretreated (for 24 h), 3D-cultured LNCaP cells ($n = 5$ for each). **: $p < 0.01$ vs. '2D'; ##: $p < 0.01$ vs. vehicle control.

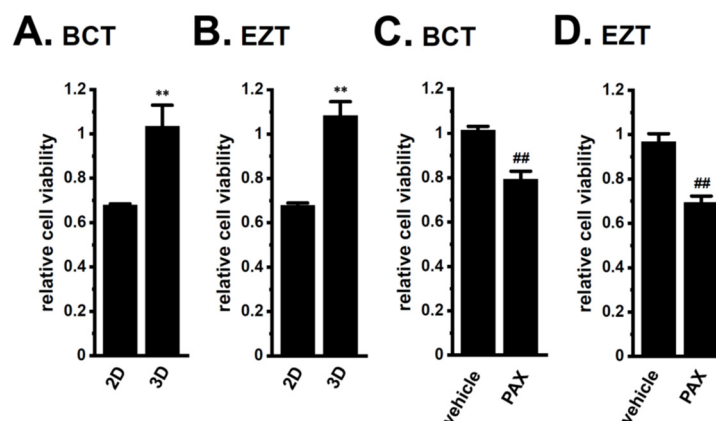


Figure 4. Effects of antiandrogens on the viability of 2D- and 3D-cultured LNCaP cells and the effects of a $K_{Ca}1.1$ inhibitor on the antiandrogen resistance acquired by 3D-cultured LNCaP cells. (A,B): Effects of the treatment with 10 μ M BCT and 10 μ M EZT for 48 h on the viability of '2D'- and '3D'-cultured LNCaP cells using the WST-1 assay ($n = 5$ for each). Cell viability adding 0.1% DMSO instead of antiandrogens was expressed as 1.0. (C,D): Effects of the treatment with antiandrogens for 48 h on the viability of vehicle- and 10 μ M PAX-pretreated (for 24 h), 3D-cultured LNCaP cells ($n = 5$ for each). **: $p < 0.01$ vs. '2D'; ##: $p < 0.01$ vs. vehicle control.

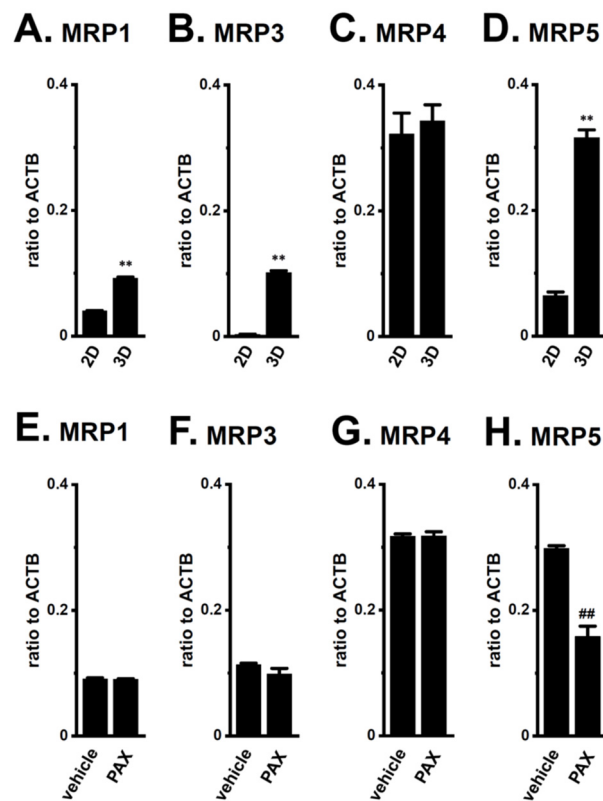


Figure 5. Expression of MRP transcripts in both 2D- and 3D-cultured LNCaP cells and the effects of $K_{Ca}1.1$ blockade with PAX on their expression in 3D-cultured LNCaP cells. (A–D): Real-time PCR examination of MRP1 (A), MRP3 (B), MRP4 (C), and MRP5 (D) in ‘2D’ monolayers and ‘3D’ spheroids of LNCaP cells ($n = 4$ for each). (E–H): Real-time PCR examination of MRP transcripts in vehicle- and PAX-treated, 3D-cultured LNCaP cells ($n = 4$ for each). Expression levels were shown as a ratio to ACTB. **: $p < 0.01$ vs. ‘2D’; #: $p < 0.01$ vs. vehicle control.

Furthermore, a co-treatment with the MRP4/5 inhibitor, MK571 and DOX overcame DOX resistance in LNCaP spheroids, whereas that with the selective MRP4 inhibitor, ceefourin 1 and DOX, did not (Figure 6C,G). Neither inhibitor overcame resistance to the other chemotherapy drugs (Figure 6). No significant changes in cell viability were observed with single treatments with MK571 or ceefourin 1 for 48 h (0.973 ± 0.031 and 0.965 ± 0.045 , respectively, in relative cell viability ($n = 5$, $p > 0.05$)). These results strongly suggest that MRP5 plays a critical role in the acquisition and $K_{Ca}1.1$ inhibition-induced overcoming of resistance by LNCaP spheroids to DOX.

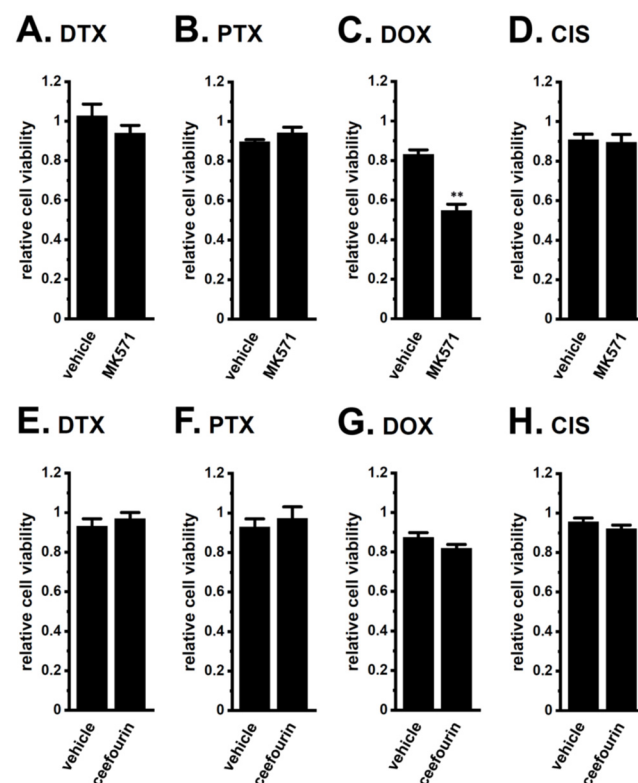


Figure 6. Effects of the MRP4/MRP5 inhibitor, MK571, and the selective MRP4 inhibitor, ceefourin 1, on chemoresistance acquired by 3D-cultured LNCaP cells. (A–D): Effects of the treatment with chemotherapy agents for 48 h on the viability of vehicle- and 10 μ M MK571-cotreated, 3D-cultured LNCaP cells ($n = 5$ for each). (E–H): Effects of the treatment with chemotherapy agents for 48 h on the viability of vehicle- and 10 μ M ceefourin 1-cotreated, 3D-cultured LNCaP cells ($n = 5$ for each). **: $p < 0.01$ vs. vehicle control.

2.3. Decreases in AR Protein Expression in Antiandrogen-Resistant-LNCaP Spheroids

We compared the gene and protein expression levels of AR between 2D monolayers and 3D spheroids of LNCaP cells using real-time PCR and WB examinations. The protein expression level of AR with a molecular weight of approximately 110 kDa decreased in lipid-raft fractions of LNCaP spheroids ($p < 0.01$) (Figure 7B,C), without changes in that of AR transcripts ($p > 0.05$) (Figure 7A). Consistent with the acquisition of resistance to antiandrogens being overcome by the PAX treatment (Figure 4), a pretreatment with 10 μ M PAX significantly increased AR protein levels in LNCaP spheroids ($p < 0.01$) (Figure 7E,F), without changes in AR transcript levels ($p > 0.05$) (Figure 7D). The MRP4/5 inhibitor, MK571, did not overcome resistance to antiandrogens by LNCaP spheroids (Supplementary Figure S3E,F). These results suggest that AR protein degradation plays a role in the acquisition of antiandrogen resistance in LNCaP spheroids, and that $K_{Ca}1.1$ inhibitors may prevent the activity and/or expression of E3s involved in AR degradation-mediated antiandrogen resistance by PCSCs.

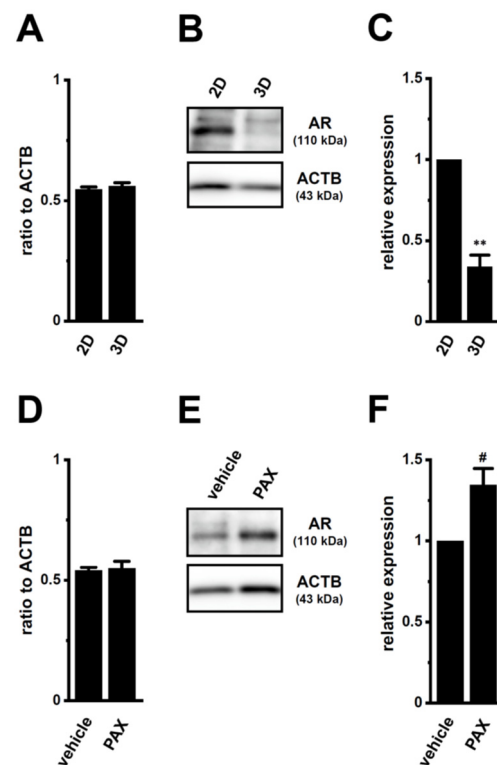


Figure 7. Decrease in AR protein expression by spheroid formation in LNCaP cells, and its reversal by the PAX treatment. (A,D): Real-time PCR examination of AR transcripts in 2D- and 3D-cultured LNCaP cells (A) and in vehicle- and PAX-treated (10 μ M) (for 24 h), 3D-cultured LNCaP cells (D) ($n = 4$ for each). Expression levels are shown as a ratio to ACTB. (B,E): AR protein expression in protein lysates from lipid-raft-enriched fractions of 2D- and 3D-cultured LNCaP cells (B) and vehicle- and PAX-treated 3D-cultured LNCaP cells (E) ($n = 4$ for each). Blots were probed with anti-AR (approximately 110 kDa, upper panel) and anti-ACTB (43 kDa, lower panel) antibodies. (C,F): Summarized results were obtained as the optical density of AR and ACTB band signals, respectively ($n = 4$ for each). After compensation for the optical density of the AR protein band signal with that of the ACTB signal, the AR signal in '2D' (C) or 'vehicle' (F) was expressed as 1.0 ($n = 4$ for each). **: $p < 0.01$ vs. '2D'; #: $p < 0.05$ vs. vehicle control.

2.4. Decrease in the Expression of the AR-Targeted Ubiquitin E3 Ligase, MDM2, in LNCaP Spheroids

Several E3s that degrade the AR protein have been identified in PC cells: SKP2 (S-phase kinase-associated protein 2), RNF6 (RING (really interesting new gene) finger protein 6), UBE3A (ubiquitin protein ligase E3A), SIAH2 (seven in absentia (*Drosophila*) homolog 2), CRBN, MDM2, NRIP (nuclear receptor interaction protein), and USP14 (ubiquitin-specific protease 14) [22–24,29]. The transcriptional expression levels of six candidates, except for MDM2 and CRBN, was not downregulated by the PAX treatment for 24 h (Supplementary Figure S5). Moreover, the expression levels of the MDM2 and CRBN transcripts and proteins were inversely correlated with AR protein expression (2D vs. 3D, Figure 8A–E; vehicle-treated vs. PAX-treated, Figure 8F–J).

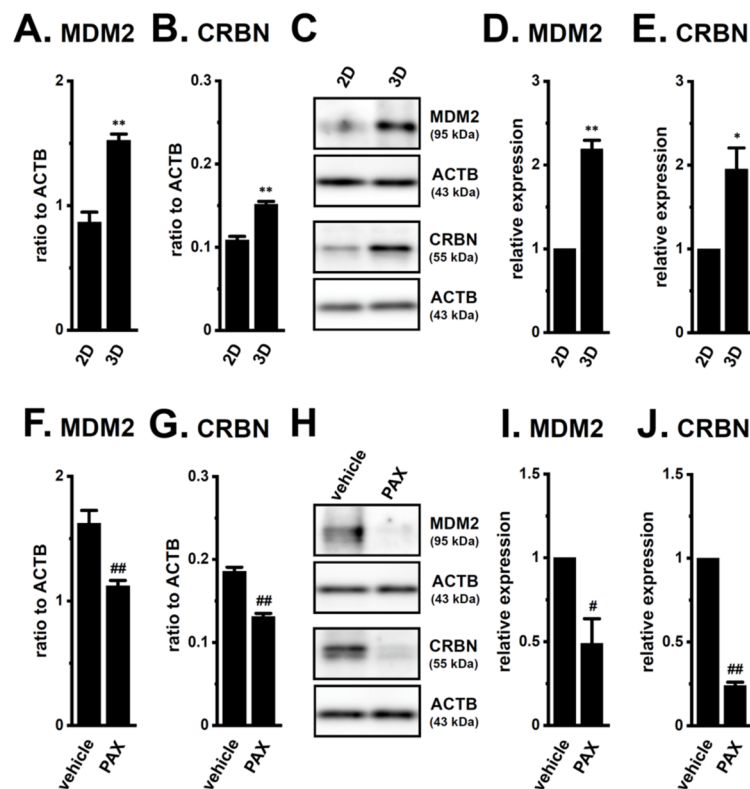


Figure 8. Comparison of expression levels of ubiquitin E3 ligases (MDM2 and CRBN) for AR between 2D- and 3D-cultured LNCaP cells, and effects of the PAX treatment in 3D-cultured LNCaP cells. (A,B): Real-time PCR examination of MDM2 (A) and CRBN (B) in '2D'- and '3D'-cultured LNCaP cells ($n = 4$ for each). Expression levels were shown as a ratio to ACTB. (C): Protein expression of MDM2 and CRBN in protein lysates from lipid-raft-enriched protein fractions of '2D'- and '3D'-cultured LNCaP cells. Blots were probed with anti-MDM2 (approximately 95 kDa), anti-CRBN (approximately 55 kDa), and anti-ACTB (43 kDa) antibodies. (D,E): Summarized results were obtained as the optical densities of MDM2 (D) and CRBN (E) band signals from 'C'. After compensation for the optical densities of the protein band signals with that of the ACTB signal, the optical density in '2D' was expressed as 1.0 ($n = 4$ for each). (F,G): Real-time PCR examination for MDM2 (F) and CRBN (G) in vehicle- and PAX-treated (10 μ M) (for 24 h) LNCaP cells ($n = 4$ for each). (H): Protein expression of MDM2 and CRBN in protein lysates from lipid-raft-enriched protein fractions of vehicle- and PAX-treated LNCaP cells. (I,J): Summarized results were obtained as the optical densities of MDM2 (I) and CRBN (J) band signals from 'H' ($n = 4$ for each). *, **: $p < 0.05$. 0.01 vs. '2D'; #, ##: $p < 0.05$. 0.01 vs. vehicle control.

To elucidate the roles of CRBN and MDM2 in antiandrogen resistance through the promotion of AR protein degradation in LNCaP spheroids, we examined the effects of the pharmacological and siRNA-mediated inhibition of CRBN and MDM2 on acquired antiandrogen resistance. A pretreatment with the MDM2 inhibitor, nutlin-3a, for 24 h significantly reversed the resistance to BCT and EZT in LNCaP spheroids ($p < 0.01$) (Figure 9A), whereas that with the CRBN inhibitor, iberdomide, did not ($p > 0.05$) (Figure 9B). Similarly, the siRNA-mediated inhibition of MDM2 reversed the resistance to antiandrogens in LNCaP spheroids ($p < 0.01$) (Figure 9C), whereas that of siRNA-mediated CRBN inhibition did not ($p > 0.05$) (Figure 9D). Correspondingly, the siRNA-mediated inhibition of MDM2, but not CRBN, significantly increased AR protein levels in LNCaP spheroids ($p < 0.05$ in si-MDM2; $p > 0.05$ in si-CRBN) (Figure 9E–H). These results strongly suggest that MDM2 is responsible for the antiandrogen resistance induced by spheroid formation in LNCaP cells through the promotion of AR protein degradation, and also that the transcriptional

repression of MDM2 mediated by the inhibition of $K_{Ca}1.1$ overcame the antiandrogen resistance acquired by LNCaP spheroids through the increase in AR protein levels.

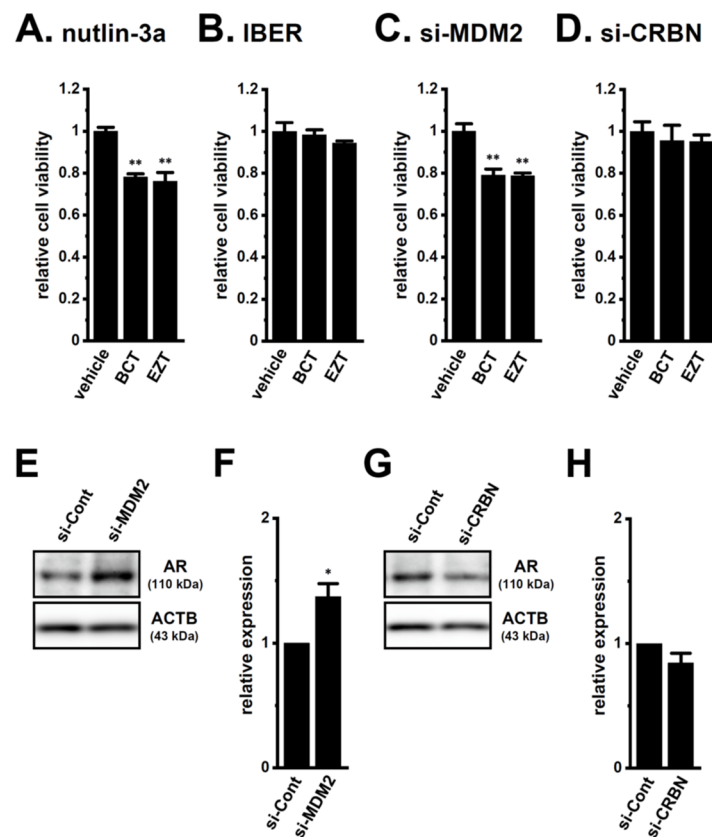


Figure 9. Effects of the pharmacological and siRNA-mediated inhibition of MDM2 and CRBN on the resistance to antiandrogens and AR protein expression in LNCaP spheroids. (**A,B**): Effects of the treatment with BCT and EZT (10 μ M) for 48 h on the viability of 2 μ M nutlin-3a- and 1 μ M iberdomide (IBER)-pretreated (for 24 h) LNCaP spheroid cells ($n = 5$ for each). (**C,D**): Effects of the treatment with antiandrogens for 48 h on the viability of MDM2 siRNA (si-MDM2)- and CRBN siRNA (si-CRBN)-transfected, 3D-cultured LNCaP cells ($n = 5$ for each). (**E,G**): Effects of the siRNA-mediated MDM2 and CRBN inhibition on AR protein expression in protein lysates from the lipid-raft-enriched fraction of LNCaP spheroids. Blots were probed with anti-AR (approximately 110 kDa, upper panel) and anti-ACTB (43 kDa, lower panel) antibodies in the control siRNA (si-Cont)-, si-MDM2-, and si-CRBN-transfected groups. (**F,H**): Summarized results were obtained as the optical density of AR and ACTB band signals in si-Cont-, si-MDM2 (F)-, and si-CRBN (H)-transfected groups ($n = 4$ for each). After compensation for the optical density of the AR protein band signal with that of the ACTB signal, the AR signal in 'si-Cont' was expressed as 1.0 ($n = 4$ for each). *, **: $p < 0.05, 0.01$ vs. vehicle control and si-Cont.

2.5. Involvement of the Ubiquitin E3 Ligase, FBXW7, in Enhancements in $K_{Ca}1.1$ Activity Induced by LNCaP Spheroid Formation

FBXW7 promoted the protein degradation of $K_{Ca}1.1$ in human breast cancer and sarcoma cell lines [18,21]. The protein expression levels of FBXW7 were markedly decreased by LNCaP spheroid formation ($p < 0.01$) (Figure 10A,B), and the siRNA-mediated inhibition of FBXW7 significantly increased the protein expression levels of $K_{Ca}1.1$ in 2D-cultured LNCaP cells ($p < 0.05$) (Figure 10C,D). These results suggest that FBXW7 plays a role in $K_{Ca}1.1$ protein degradation in LNCaP cells.

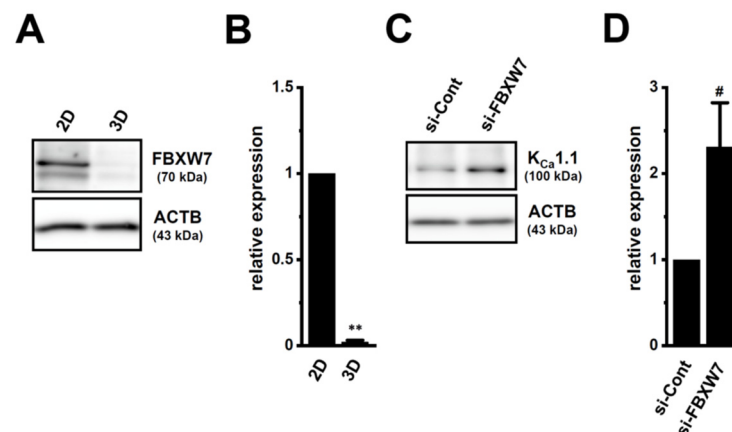


Figure 10. Regulation of $K_{Ca}1.1$ protein degradation through the FBXW7 ubiquitin E3 ligase in LNCaP cells. (A,B) Protein expression of FBXW7 in whole cell protein lysates of ‘2D’- and ‘3D’-cultured LNCaP cells. Blots were probed with anti-FBXW7 (approximately 70 kDa) and anti-ACTB (43 kDa) antibodies (A). Summarized results (B) were obtained as the optical densities of FBXW7 and ACTB band signals ($n = 4$ for each). After compensation for the optical densities of the protein band signals with that of the ACTB signal, the optical density in ‘2D’ was expressed as 1.0 ($n = 4$ for each). (C,D): Protein expression of $K_{Ca}1.1$ in control siRNA (si-Cont)- and FBXW7 siRNA (si-FBXW7)-transfected (for 72 h), 2D-cultured LNCaP cells. Blots were probed with anti- $K_{Ca}1.1$ (approximately 100 kDa) and anti-ACTB (43 kDa) antibodies (C). Summarized results (D) were obtained as the optical densities of $K_{Ca}1.1$ and ACTB band signals. The optical density in ‘si-Cont’ was expressed as 1.0 ($n = 4$ for each). **: $p < 0.01$ vs. ‘2D’; #: $p < 0.05$ vs. ‘si-Cont’.

3. Discussion

Recent studies demonstrated that K^+ channels are important contributors to drug resistance being overcome in solid cancers [14,30]. $K_{Ca}1.1$ gene amplification plays an important role in PC progression [15]. The main results of the present study are as follows: (1) the inhibition of $K_{Ca}1.1$ overcame acquired resistance to antiandrogens in LNCaP spheroids (Figure 4); (2) AR protein degradation by the upregulation of MDM2 was associated with the acquisition of antiandrogen resistance in LNCaP spheroids, and the pharmacological inhibition of $K_{Ca}1.1$ reversed MDM2-mediated AR degradation, which overcame antiandrogen resistance (Figures 7–9); and (3) the inhibition of $K_{Ca}1.1$ overcame acquired resistance to DOX in LNCaP spheroids (Figure 3), and MRP5 was associated with both the acquisition of DOX resistance and it being overcome by the inhibition of $K_{Ca}1.1$ (Figures 5 and 6). We also found that $K_{Ca}1.1$ proteins were overexpressed in LNCaP spheroids, together with a decrease in FBXW7-mediated $K_{Ca}1.1$ protein degradation (Figures 1 and 10). Collectively, the present results demonstrated the impact of $K_{Ca}1.1$ on the resistance to antiandrogens and DOX in LNCaP spheroid models.

The E3, MDM2, promotes cancer stemness with an AR-negative signature in PCSCs by selectively degrading AR proteins [24]. In contrast, the loss of MDM2 promotes CSC differentiation by reversing the processes of PC stemness [24]. In the present study, several PCSC markers were overexpressed by LNCaP spheroid formation (Figure 2). NANOG has been implicated in the acquisition of cancer therapy resistance [31], and its overexpression in PC cells has been shown to reduce AR levels [32]. MDM2 and CRBN were included among the 6490 target genes of the NANOG transcription factor obtained from the chromatin immunoprecipitation (ChIP) enrichment analysis (ChEP) transcriptional factor targets dataset [33]. These findings suggest that NANOG is a transcription factor of MDM2 in PCSCs; however, further studies are needed to obtain direct evidence to show that MDM2 is a NANOG downstream gene in PCSCs. Additionally, several studies have shown that signal transducer and activator of transcription (STAT) signaling pathways play critical roles in the AR protein degradation and stabilization in PC cells [34,35]. Further

studies will be needed to elucidate the possible involvement of $K_{Ca}1.1$ in the regulation of STAT pathway-mediated AR protein degradation.

The present study indicated that acquired resistance to DOX in LNCaP spheroids was due to upregulated MRP5 expression (Figures 3C and 5D). Consistent with these results, DOX resistance was reversed by a treatment with the MRP4/5 inhibitor without affecting the selective MRP4 inhibitor (Figure 6C,G). These results are in accordance with recent findings showing that MRP5 was associated with drug resistance to DOX, but not PTX or CIS [26,36]. Different from our recent study on sarcoma spheroids [21], the inhibition of $K_{Ca}1.1$ did not affect the expression levels of MRP1 (Figure 5E) and Nrf2 (Supplementary Figure S6A) in LNCaP spheroids. In fibrosarcoma spheroids, the NANOG inhibition reverses DOX resistance [31]. As shown in Supplementary Figure S6B–D, the inhibition of $K_{Ca}1.1$ downregulated the expression of the CSC markers in LNCaP spheroids. It currently remains unclear whether MRP5 is a NANOG downstream gene in PCSCs; however, it was not included among the 6490 target genes of the NANOG transcription factor obtained from the ChEP transcriptional factor targets dataset. Furthermore, Ji et al. (2021) recently showed that the high expression of MRP5 reduced the sensitivity of LNCaP spheroids to EZT [37]. However, the present study showed no significant changes in antiandrogen resistance in LNCaP spheroids treated with MK571 (Supplementary Figure S3E,F).

Consistent with human sarcoma spheroid models [21], $K_{Ca}1.1$ protein degradation was suppressed by the downregulation of FBXW7 in LNCaP spheroids (Figure 10) [21]. Recent studies have focused on the role of mitochondrial ion channels in chemoresistance in cancers [38,39]. Mitochondrial $K_{Ca}1.1$ may be responsible for the acquisition of resistance to antiandrogens and chemotherapies by PCSCs. A more detailed understanding of $K_{Ca}1.1$ -regulated resistance to antiandrogens and chemotherapies is needed for the development of novel treatment strategies for CRPCs associated with PCSCs.

The pro-inflammatory cytokines, IL-1 β and IL-8, have been shown to repress AR mRNA expression in PC cells [40,41], and play a role in antiandrogen resistance in PC [42]. However, their levels in LNCaP spheroids were undetectable by an ELISA assay (less than 1 pg/mg protein). As shown in Figure 7D, the inhibition of $K_{Ca}1.1$ in LNCaP spheroids did not affect the expression level of AR; however, IL-1 β and/or IL-8-producing, tumor-infiltrating non-cancerous cells, such as tumor-associated macrophages cells in the TME, may be responsible for the AR transcriptional repression-mediated antiandrogen resistance in PCSCs.

In the TME of PC, tumor-infiltrating, non-cancerous cells, such as regulatory T cells, tumor-associated macrophages (TAMs), myeloid-derived suppressor cells (MDSCs), and cancer-associated fibroblasts (CAFs), play a critical role in immunosuppression [43]. A recent study showed that AR-expressing CAFs can affect PC progression and metastasis [44]. In addition, TAM-derived IL-6 and IL-8 are important for the regulation of AR expression and antiandrogen resistance [44]. Studies to shed light on the cellular heterogeneity of TME using accurate TME-mimicking cancer organoid models and patient-derived organoids will be needed to elucidate more mechanisms underlying AR protein degradation and antiandrogen resistance in PCSCs.

4. Materials and Methods

4.1. Materials and Reagents

The following chemicals and reagents were used: EZT, iberdomide, MK571 (MedChemExpress, Monmouth Junction, NJ, USA), BCT (Adooq Bioscience, Irvine, CA, USA), PAX, nutlin-3a (Cayman Chemical, Ann Arbor, MI, USA), NS1619, ceefourin 1 (Abcam, Cambridge, UK), docetaxel (DTX) (TCL, Tokyo, Japan), PTX, DOX hydrochloride, CIS, RPMI 1640 medium (FUJIFILM, Osaka, Japan), DiBAC₄(3), WST-1 (Dojindo, Kumamoto, Japan), Select Pre-designed/Validated siRNAs as a negative control (Pre-designed, No. 1), CRBN (Pre-designed, ID#: s534902), FBXW7 (Pre-designed, ID#: s224356), MDM2 (Validated, ID#: s8630) and Lipofectamine[®] RNAiMAX (Thermo Fisher Scientific, Waltham, MA, USA), and ReverTra Ace (ToYoBo, Osaka, Japan). The other chemicals used in the

present study were from Sigma-Aldrich (St. Louis, MO, USA), FUJIFILM, and Nacalai Tesque (Kyoto, Japan), unless otherwise stated.

4.2. Cell Culture

The human PC LNCaP cell line was purchased from the RIKEN Cell Bank (Osaka, Japan). They were cultured in RPMI 1640 medium supplemented with 10 nM dihydrotestosterone, 10% fetal bovine serum, and a penicillin–streptomycin mixture. The cells were cultured at 37 °C in a humidified atmosphere containing 5% CO₂. Flat-bottomed dishes and plates (Corning, Corning, NY, USA) were used for the 2D cell culture [21]. The PrimeSurface[®] system (Sumitomo Bakelite, Tokyo, Japan) was used for the 3D spheroid culture. LNCaP cell suspensions were seeded onto a PrimeSurface 96U plate at 10⁵ cells/well, and then cultured for 7 days.

4.3. Real-Time PCR

Total RNA was isolated from cancer cells using the conventional acid guanidinium thiocyanate-phenol-chloroform extraction method. The concentration and quality of RNA were confirmed using the microvolume spectrophotometer, NanoDrop One (Thermo Fisher Scientific). Reverse transcription was performed using ReverTra Ace with random hexanucleotides. Quantitative, real-time PCR was conducted using the Luna Universal qPCR Master Mix (New England Biolabs Japan, Tokyo, Japan) and the Applied Biosystems 7500 Fast Real-Time PCR System (Thermo Fisher Scientific). PCR primers of human origin were listed in Supplementary Scheme S1. Relative expression levels were calculated using the 2^{-ΔΔCt} method [21] and normalized to ACTB.

4.4. Measurements of K_{Ca}1.1 Activity by Voltage-Sensitive Dye Imaging and Whole-Cell Patch Clamp Recordings

Membrane potential was measured using the fluorescent voltage-sensitive dye DiBAC₄(3) [18,21]. Briefly, prior to fluorescence measurements, the cells were incubated in normal 2-[4-(2-Hydroxyethyl)-1-piperazinyl]ethanesulfonic acid (HEPES) buffer containing 100 nM DiBAC₄(3) at room temperature for 20 min, and the cells were then continuously incubated in 100 nM DiBAC₄(3) throughout the experiments. Hyperpolarizing responses induced by the K_{Ca}1.1 activator, NS1619 (1 μM) (decrease in fluorescence intensity), were measured using an ORCA-Flash2.8 digital camera (Hamamatsu Photonics, Hamamatsu, Japan). Data collection and analyses were performed using the HImage system (Hamamatsu Photonics). Images were measured every 5 s.

A whole-cell patch clamp was applied to 3D-cultured LNCaP cells using the Axon Patch Clamp System (Axopatch 200B amplifier, Molecular Devices, San Jose, CA, USA) at room temperature (23 ± 1 °C). Data acquisition and analyses of whole cell currents were performed using Axon Digidata 1550B plus HumSilencer and Axon pCLAMP Software Suite (Molecular Devices). Whole-cell currents were measured in the voltage-clamp mode and induced by 500-ms voltage steps, every 15 s, from -80 to +60 mV at a holding potential of -60 mV. The external solution was (in mM): 137 NaCl, 5.9 KCl, 2.2 KCl, 1.2 MgCl₂, 14 glucose, and 10 HEPES, pH7.4. The pipette solution was (in mM): 140 KCl, 4 MgCl₂, 3.2 CaCl₂, 5 EGTA, 10 HEPES, and 2 Na₂ATP, pH 7.2, with an estimated free Ca²⁺ concentration of 100 nM (pCa 7.0).

4.5. Western Blotting

Whole cell lysates were extracted using a radioimmunoprecipitation (RIPA) buffer. Lipid-raft-enriched protein fraction lysates were extracted using the ULTRARIPA kit for Lipid Rafts (BioDynamics Laboratory, Tokyo, Japan), according to the manufacturer's instructions. Equal amounts of protein were subjected to SDS-PAGE and immunoblotting with anti-K_{Ca}1.1 polyclonal (rabbit) (approximately 100 kDa) (1:750, APC-021, Alomone Labs, Jerusalem, Israel), anti-AR polyclonal (rabbit) (approx. 110 kDa) (1:750, C-19, Santa Cruz Biotechnology, SCB, Santa Cruz, CA, USA), anti-FBXW7 polyclonal (rabbit) (approx. 70 kDa) (1:2000, ABclonal, Tokyo, Japan), anti-CRBN polyclonal (rabbit) (approx. 55 kDa)

(1:1500, ABclonal), anti-MDM2 polyclonal (rabbit) (approx. 95 kDa) (1:2000, ABclonal), anti-MRP1 polyclonal (rabbit) (approx. 250 kDa) (1:1500, Bioss Antibodies, Woburn, MA, USA), anti-MRP3 polyclonal (rabbit) (approx. 170 kDa) (1:1000, ABclonal), anti-MRP4 polyclonal (rabbit) (160–200 kDa) (1:2000, ABclonal), anti-MRP5 polyclonal (rabbit) (approx. 160 kDa) (1:1500, ABclonal), and anti-ACTB monoclonal (mouse) (43 kDa) (1:15,000, 6D1, Medical & Biological Laboratories, Nagoya, Japan) antibodies, and then incubated with anti-rabbit and mouse horseradish peroxidase-conjugated IgG (Merck Millipore, Darmstadt, Germany). Strong band signal for flotillin-1 (45 kDa, anti-flotillin polyclonal (rabbit) antibody, GeneTex, Alton Pkwy Irvine, CA, USA) protein, a lipid-raft marker, was detected in ultra-RIPA soluble fractions, but not RIPA soluble ones. Image detections and the quantitative analyses of the optical densities of protein band signals were performed as previously reported [21].

4.6. Immunocytochemistry

Fixed and non-permeabilized cells were stained with an anti-K_{Ca}1.1 (extracellular) polyclonal antibody (rabbit) (APC-151, Alomone Labs) followed by an Alexa Fluor 488-conjugated secondary antibody (Thermo Fisher Scientific), and then analyzed by flow cytometry (FACSCanto II, BD Biosciences, San Jose, CA, USA). K_{Ca}1.1 expression was expressed as means fluorescence intensity after the subtraction of that in cells stained by the secondary antibody [21].

4.7. Cell Viability Assay

Cell viability was assessed using the WST-1 assay [21]. Briefly, using a density of 10⁵ cells/mL, cells were cultured in duplicate in 96-well plates for 7 days (for the 3D culture) and 1 day (for the 2D culture). The cells were then treated with drugs used in chemotherapy (DTX, PTX, DOX, and CIS) and antiandrogens (BCT and EZT) for 48 h. Two hours after the addition of WST-1 reagent to each well, the absorbance was measured using the microplate reader SpectraMax 384 (Molecular Devices Japan, Tokyo, Japan) at a test wavelength of 450 nm and reference wavelength of 650 nm.

4.8. Targeted Gene Suppression by siRNA Transfection

Lipofectamine[®] RNAiMAX reagent (Thermo Fisher Scientific) was used in the siRNA-mediated blockade of FBXW7, CRBN, and MDM2 according to the manufacturer's protocol. Silencer Select Pre-designed/Validated siRNAs for the negative control (No. 1) (si-Cont), FBXW7 (si-FBXW7), CRBN (si-CRBN), and MDM2 (si-MDM2) were transfected into adherent monolayer LNCaP cells. Twenty-four hours later, si-CRBN- and si-MDM2-transfected cells were seeded onto PrimeSurface 96U. The expression levels of the target transcripts were assessed 3 days (for si-FBXW7 transfectant) and 7 days (for si-CRBN and si-MDM2 transfectants) after transfection using real-time PCR assay, resulting in more than 70% reduction.

4.9. Statistical Analysis

Statistical evaluation was performed with Statistical software XLSTAT (version 2013.1). Unpaired/paired Student's *t*-tests with Welch's correction or Tukey's tests were used to assess the significance of differences between two groups and among multiple groups. Results with a *p* value of less than 0.05 were considered to be significant. Data were presented as means ± SEM.

5. Conclusions

In conclusion, the present results suggest that K_{Ca}1.1 may be a key modulator of antiandrogen resistance in androgen-sensitive, K_{Ca}1.1 gene-amplified PC, and that K_{Ca}1.1 inhibitors may overcome acquired antiandrogen resistance in PCSCs. Furthermore, K_{Ca}1.1 played a vital role in the overcome of DOX resistance by downregulating MRP5 in LNCaP spheroids, suggesting the potential of K_{Ca}1.1 inhibitors as an effective therapeutic inter-

vention in combination with antiandrogens. The targeting of K_{Ca}1.1 is promising for suppressing the progression of CRPC associated with PCSCs through the regulation of MDM2-mediated AR degradation.

Supplementary Materials: The following are available online at <https://www.mdpi.com/article/10.3390/ijms222413553/s1>.

Author Contributions: Conceptualization, S.O. and J.K.; validation, S.O. and J.K.; formal analysis, S.O., J.K., H.K. and K.E.; investigation, S.O., J.K., H.K., K.E. and M.M.; data curation, S.O., J.K., H.K. and K.E.; writing—original draft preparation, S.O. and J.K.; writing—review and editing, S.O., J.K., H.K., K.E. and M.M.; funding acquisition, S.O. All authors have read and agreed to the published version of the manuscript.

Funding: This research was funded by JSPS KAKENHI Grants [JP20K07071] (S.O.).

Institutional Review Board Statement: Not applicable.

Informed Consent Statement: Not applicable.

Acknowledgments: Medical English Service (Kyoto, Japan) reviewed the manuscript prior to submission.

Conflicts of Interest: The authors declare no conflict of interest.

References

- Damodaran, S.; Lang, J.M.; Jarrard, D.F. Targeting metastatic hormone sensitive prostate cancer. Chemohormonal therapy and new combinatorial approaches. *J. Urol.* **2019**, *201*, 876–885. [[CrossRef](#)] [[PubMed](#)]
- Wang, Y.; Chen, J.; Wu, Z.; Ding, W.; Gao, S.; Gao, Y.; Xu, C. Mechanisms of enzalutamide resistance in castration-resistant prostate cancer and therapeutic strategies to overcome it. *Br. J. Pharmacol.* **2021**, *178*, 239–261. [[CrossRef](#)] [[PubMed](#)]
- Rice, M.A.; Malhotra, S.V.; Stoyanova, T. Second-generation antiandrogens: From discovery to standard of care in castration resistant prostate cancer. *Front. Oncol.* **2019**, *9*, 801. [[CrossRef](#)] [[PubMed](#)]
- Nakazawa, M.; Paller, C.; Kyprianou, N. Mechanisms of therapeutic resistance in prostate cancer. *Curr. Oncol. Rep.* **2017**, *19*, 13. [[CrossRef](#)]
- Zazzo, E.D.; Galasso, G.; Giovannelli, P.; Donato, M.D.; Santi, A.D.; Cerner, G.; Rossi, V.; Abbondanza, C.; Monchamont, B.; Sinisi, A.A.; et al. Prostate cancer stem cells: The role of androgen and estrogen receptors. *Oncotarget* **2016**, *7*, 193–208. [[CrossRef](#)]
- Powers, E.; Karachaliou, G.S.; Kao, C.; Harrison, M.R.; Hoimes, C.J.; George, D.J.; Armstrong, A.J.; Zhang, T. Novel therapies are changing treatment paradigms in metastatic prostate cancer. *J. Hematol. Oncol.* **2020**, *13*, 144. [[CrossRef](#)] [[PubMed](#)]
- Shehzad, A.; Ravinayagam, V.; AlRumaih, H.; Aljafary, M.; Almohazey, D.; Almoftay, S.; Al-Rashid, N.A.; Al-Suhaimi, E.A. Application of three-dimensional (3D) tumor cell culture systems and mechanism of drug resistance. *Curr. Pharm. Des.* **2019**, *25*, 3599–3607. [[CrossRef](#)]
- Costa, E.C.; Moreira, A.F.; de Melo-Diogo, D.; Gaspar, V.M.; Carvalho, M.P.; Correia, I.J. 3D tumor spheroids: An overview on the tools and techniques used for their analysis. *J. Biotechnol. Adv.* **2016**, *34*, 1427–1441. [[CrossRef](#)]
- Zadvornyi, T.V.; Lukianova, N.Y.; Borikun, T.V.; Vitruk, Y.V.; Stakhovsky, E.O.; Chekhun, V.F. NANOG as prognostic factor of prostate cancer course. *Exp. Oncol.* **2020**, *42*, 94–100. [[CrossRef](#)] [[PubMed](#)]
- Huang, C.; Yoon, C.; Zhou, X.H.; Zhou, Y.C.; Zhou, W.W.; Liu, H.; Yang, X.; Lu, J.; Lee, S.Y.; Huang, K. ERK1/2-Nanog signaling pathway enhances CD44⁺ cancer stem-like cell phenotypes and epithelial-to-mesenchymal transition in head and neck squamous cell carcinomas. *Cell Death Dis.* **2020**, *11*, 266. [[CrossRef](#)] [[PubMed](#)]
- Prevarskaya, N.; Skryma, R.; Shuba, Y. Ion channels in cancer: Are cancer hallmarks oncochannelopathies? *Physiol. Rev.* **2018**, *98*, 559–621. [[CrossRef](#)]
- Cheng, Q.; Chen, A.; Du, Q.; Liao, Q.; Shuai, Z.; Chen, C.; Yang, X.; Hu, Y.; Zhao, J.; Liu, S.; et al. Novel insights into ion channels in cancer stem cells (Review). *Int. J. Oncol.* **2018**, *53*, 1435–1441. [[CrossRef](#)]
- Girault, A.; Ahidouch, A.; Ouadid-Ahidouch, H. Roles for Ca²⁺ and K⁺ channels in cancer cells exposed to the hypoxic tumour microenvironment. *Biochim. Biophys. Acta Mol. Cell Res.* **2020**, *1867*, 118644. [[CrossRef](#)]
- Kischel, P.; Girault, A.; Rodat-Despoix, L.; Chamli, M.; Radoslovova, S.; Abou Daya, H.; Lefebvre, T.; Foulon, A.; Rybarczyk, P.; Hague, F.; et al. Ion channels: New actors playing in chemotherapeutic resistance. *Cancers* **2019**, *11*, 376. [[CrossRef](#)]
- Bailey, C.S.; Moldenhauer, H.J.; Park, S.M.; Keros, S.; Meredith, A.L. KCNMA1-linked channelopathy. *J. Gen. Physiol.* **2019**, *151*, 1173–1189. [[CrossRef](#)]
- Du, C.; Zheng, Z.; Li, D.; Chen, L.; Li, N.; Yi, X.; Yang, Y.; Guo, F.; Liu, W.; Xie, X.; et al. BKCa promotes growth and metastasis of prostate cancer through facilitating the coupling between $\alpha v \beta 3$ integrin and FAK. *Oncotarget* **2016**, *7*, 40174–40188. [[CrossRef](#)]
- Basile, M.S.; Fagone, P.; Mangano, K.; Mammana, S.; Magro, G.; Salvatorelli, L.; Li Destri, G.; La Greca, G.; Nicoletti, F.; Puleo, S.; et al. KCNMA1 expression is downregulated in colorectal cancer via epigenetic mechanisms. *Cancers* **2019**, *11*, 245. [[CrossRef](#)] [[PubMed](#)]

18. Khatun, A.; Shimozawa, M.; Kito, H.; Kawaguchi, M.; Fujimoto, M.; Ri, M.; Kajikuri, J.; Niwa, S.; Fujii, M.; Ohya, S. Transcriptional repression and protein degradation of the Ca²⁺-activated K⁺ channel K_{Ca}1.1 by androgen receptor inhibition in human breast cancer cells. *Front. Physiol.* **2018**, *9*, 312. [[CrossRef](#)]
19. Gonzalez-Perez, V.; Lingle, C.J. Regulation of BK channels by β and γ subunits. *Annu. Rev. Physiol.* **2019**, *81*, 113–137. [[CrossRef](#)] [[PubMed](#)]
20. Sun, T.; Liu, Z.; Yang, Q. The role of ubiquitination and deubiquitination in cancer metabolism. *Mol. Cancer* **2020**, *19*, 146. [[CrossRef](#)] [[PubMed](#)]
21. Ohya, S.; Kajikuri, J.; Endo, K.; Kito, H.; Elboray, E.E.; Suzuki, T. Ca²⁺-activated K⁺ channel K_{Ca}1.1 as a therapeutic target to overcome chemoresistance in three-dimensional sarcoma spheroid models. *Cancer Sci.* **2021**, *112*, 3769–3783. [[CrossRef](#)] [[PubMed](#)]
22. Choi, T.Y.; Lee, S.H.; Kim, Y.J.; Bae, J.R.; Lee, K.M.; Jo, Y.; Kim, S.J.; Lee, A.R.; Choi, S.; Choi, L.M.; et al. Cereblon maintains synaptic and cognitive function by regulating BK channel. *J. Neurosci.* **2018**, *38*, 3571–3583. [[CrossRef](#)]
23. Takwale, A.D.; Jo, S.H.; Jeon, Y.U.; Kim, H.S.; Shin, C.H.; Lee, H.K.; Ahn, S.; Lee, C.O.; Ha, J.D.; Kim, J.H.; et al. Design and characterization of cereblon-mediated androgen receptor proteolysis-targeting chimeras. *Eur. J. Med. Chem.* **2020**, *208*, 112769. [[CrossRef](#)]
24. Vummidi Giridhar, P.; Williams, K.; VonHandorf, A.P.; Deford, P.L.; Kasper, S. Constant degradation of the androgen receptor by MDM2 conserves prostate cancer stem cell integrity. *Cancer Res.* **2019**, *79*, 1124–1137. [[CrossRef](#)] [[PubMed](#)]
25. Xiao, H.; Zheng, Y.; Ma, L.; Tian, L.; Sun, Q. Clinically-relevant ABC transporter for anti-cancer drug resistance. *Front. Pharmacol.* **2021**, *12*, 648407. [[CrossRef](#)] [[PubMed](#)]
26. Wang, J.Q.; Yang, Y.; Cai, C.Y.; Teng, Q.X.; Cui, Q.; Lin, J.; Assaraf, Y.G.; Chen, Z.S. Multidrug resistance proteins (MRPs): Structure, function and the overcoming of cancer multidrug resistance. *Drug Resist. Updates* **2021**, *54*, 100743. [[CrossRef](#)] [[PubMed](#)]
27. Yan, J.; Aldrich, R.W. LRRC26 auxiliary protein allows BK channel activation at resting voltage without calcium. *Nature* **2010**, *466*, 513–516. [[CrossRef](#)]
28. Narusaka, T.; Ohara, T.; Noma, K.; Nishiwaki, N.; Katsura, Y.; Kato, T.; Sato, H.; Tomono, Y.; Kikuchi, S.; Tazawa, H.; et al. Nanog is a promising chemoresistant stemness marker and therapeutic target by iron chelators for esophageal cancer. *Int. J. Cancer* **2021**, *149*, 347–357. [[CrossRef](#)] [[PubMed](#)]
29. Li, B.; Lu, W.; Chen, Z. Regulation of androgen receptor by E3 ubiquitin ligases: For more or less. *Recept. Clin. Investig.* **2014**, *1*, e122. [[CrossRef](#)]
30. Ramírez, A.; García-Quiroz, J.; Aguilar-Eslava, L.; Sanchez-Pérez, Y.; Camacho, J. Novel therapeutic approaches of ion channels and transporters in cancer. In *Reviews of Physiology, Biochemistry and Pharmacology*; Springer: Berlin, Germany, 2020; Volume 177, pp. 1–57.
31. Yoon, C.; Lu, J.; Yi, B.C.; Chang, K.K.; Simon, M.C.; Ryeom, S.; Yoon, S.S. PI3K/Akt pathway and Nanog maintain cancer stem cells in sarcomas. *Oncogenesis* **2021**, *10*, 12. [[CrossRef](#)] [[PubMed](#)]
32. Jeter, C.R.; Liu, B.; Lu, Y.; Chao, H.P.; Zhang, D.; Liu, X.; Chen, X.; Li, Q.; Rycaj, K.; Calhoun-Davis, T.; et al. NANOG reprograms prostate cancer cells to castration resistance via dynamically repressing and engaging the AR/FOXA1 signaling axis. *Cell Discov.* **2016**, *2*, 16041. [[CrossRef](#)] [[PubMed](#)]
33. Rouillard, A.D.; Gunderson, G.W.; Fernandez, N.F.; Wang, Z.; Monteiro, C.D.; McDermott, M.G.; Ma'avan, A. The harmonizome: A collection of processed datasets gathered to serve and mine knowledge about genes and proteins. *Database* **2016**, *2016*, baw100. [[CrossRef](#)] [[PubMed](#)]
34. Pühr, M.; Hoefler, J.; Eigentler, A.; Dietrich, D.; van Leenders, G.; Uhl, B.; Hoogland, M.; Handle, F.; Schlick, B.; Neuwirt, H.; et al. PIAS1 is a determinant of poor survival and acts as a positive feedback regulator of AR signaling through enhanced AR stabilization in prostate cancer. *Oncogene* **2016**, *35*, 2322–2332. [[CrossRef](#)] [[PubMed](#)]
35. Thomas, C.; Zoubeydi, A.; Kuruma, H.; Fazli, L.; Lamoureux, F.; Beraldi, E.; Monia, B.P.; MacLeod, A.; Thüroff, J.W.; Gleave, M.E. Transcriptional factor Stat5 knockdown enhances androgen receptor degradation and delays castration-resistant prostate cancer progression in vivo. *Mol. Cancer Ther.* **2011**, *10*, 347–359. [[CrossRef](#)] [[PubMed](#)]
36. Pan, S.T.; Li, Z.I.; He, Z.X.; Qiu, J.X.; Zhou, S.F. Molecular mechanisms for tumour resistance to chemotherapy. *Clin. Exp. Pharmacol. Physiol.* **2016**, *43*, 723–737. [[CrossRef](#)] [[PubMed](#)]
37. Ji, G.; He, S.; Huang, C.; Gong, Y.; Li, X.; Zhou, L. Upregulation of ATP binding cassette subfamily C member 5 facilitates prostate cancer progression and enzalutamide resistance via the CDK1-mediated AR Ser81 phosphorylation pathway. *Int. J. Biol. Sci.* **2021**, *17*, 1613–1628. [[CrossRef](#)]
38. Puruzzo, R.; Szabo, I. Contribution of mitochondrial ion channels to chemo-resistance in cancer cells. *Cancers* **2019**, *11*, 761. [[CrossRef](#)]
39. Szabo, I.; Zoratti, M.; Biasutto, L. Targeting mitochondrial ion channels for cancer therapy. *Redox Biol.* **2021**, *42*, 101846. [[CrossRef](#)] [[PubMed](#)]
40. Dahl, H.C.; Kanchwala, M.; Thomas-Jardin, S.E.; Sandhu, A.; Kanmuri, P.; Nawas, A.F.; Xing, C.; Lin, C.; Frigo, D.E.; Delk, N.A. Chronic IL-1 exposure drives LNCaP cells to evolve androgen and AR independence. *PLoS ONE* **2020**, *15*, e0242970. [[CrossRef](#)] [[PubMed](#)]
41. Araki, S.; Omori, Y.; Lyn, D.; Singh, R.K.; Meinbach, D.M.; Sandman, Y.; Lokeshwar, V.B.; Lokeshwar, B.L. Interleukin-8 is a molecular determinant of androgen independence and progression in prostate cancer. *Cancer Res.* **2007**, *67*, 6854–6862. [[CrossRef](#)] [[PubMed](#)]

42. Staverosky, J.A.; Zhu, X.H.; Ha, S.; Logan, S.K. Anti-androgen resistance in prostate cancer cells chronically induced by interleukin-1 β . *Am. J. Clin. Exp. Urol.* **2013**, *1*, 53–65. [[PubMed](#)]
43. Di Donato, M.; Zamagni, A.; Galasso, G.; Di Zazzo, E.; Giovannelli, P.; Barone, M.V.; Zanoni, M.; Gunelli, R.; Costantini, M.; Auricchio, F.; et al. The androgen receptor/filamin A complex as a target in prostate cancer microenvironment. *Cell Death Dis.* **2021**, *12*, 127. [[CrossRef](#)] [[PubMed](#)]
44. Wang, G.; Zhao, D.; Spring, D.J.; DePinho, R.A. Genetics and biology of prostate cancer. *Genes Dev.* **2018**, *32*, 1105–1140. [[CrossRef](#)] [[PubMed](#)]